JACS
JOURNAL OF THE AMERICAN CHEMICAL SOCIETY
Article
pubs.acs.org/JACS

$ZnTaO_2N$: Stabilized High-Temperature $LiNbO_3$-type Structure

Yoshinori Kuno,[†] Cédric Tassel,[†,‡] Koji Fujita,[†] Dmitry Batuk,[§] Artem M. Abakumov,[∥,§] Kazuki Shitara,[⊥] Akihide Kuwabara,[⊥] Hiroki Moriwake,[⊥] Daichi Watabe,[†] Clemens Ritter,[#] Craig M. Brown,[∇] Takafumi Yamamoto,[†] Fumitaka Takeiri,[†] Ryu Abe,[†] Yoji Kobayashi,[†] Katsuhisa Tanaka,[†] and Hiroshi Kageyama*[,†,○]

[†]Graduate School of Engineering, Kyoto University, Nishikyo-ku, Kyoto 615-8510, Japan

[‡]The Hakubi Center for Advanced Research, Kyoto University, Kyoto 606-8501, Japan

[§]Electron Microscopy for Materials Research (EMAT), University of Antwerp, Groenenborgerlaan 171, 2020 Antwerpen, Belgium

[∥]Skoltech Center for Electrochemical Energy Storage, Skolkovo Institute of Science and Technology, Nobel Str. 3, 143026 Moscow, Russia

[⊥]Nanostructures Research Laboratory, Nagoya 456-8587, Japan

[#]Institute Laue-Langevin, 71 Avenue des Martyrs, 38000 Grenoble, France

[∇]Center for Neutron Research, National Institute of Standards and Technology (NIST), Gaithersburg, Maryland 20899, United States

[○]CREST, Japan Science and Technology Agency (JST), Kawaguchi, Saitama 332-0012, Japan

Supporting Information

ABSTRACT: By using a high-pressure reaction, we prepared a new oxynitride $ZnTaO_2N$ that crystallizes in a centrosymmetric ($R\bar{3}c$) high-temperature $LiNbO_3$-type structure (HTLN-type). The stabilization of the HTLN-type structure down to low temperatures (at least 20 K) makes it possible to investigate not only the stability of this phase, but also the phase transition to a noncentrosymmetric ($R3c$) $LiNbO_3$-type structure (LN-type) which is yet to be clarified. Synchrotron and neutron diffraction studies in combination with transmission electron microscopy show that Zn is located at a disordered 12*c* site instead of 6*a*, implying an order−disorder mechanism of the phase transition. It is found that the closed d-shell of Zn^{2+}, as well as the high-valent Ta^{5+} ion, is responsible for the stabilization of the HTLN-type structure, affording a novel quasitriangular ZnO_2N coordination. Interestingly, only 3% Zn substitution for $MnTaO_2N$ induces a phase transition from LN- to HTLN-type structure, implying the proximity in energy between the two structural types, which is supported by the first-principles calculations.

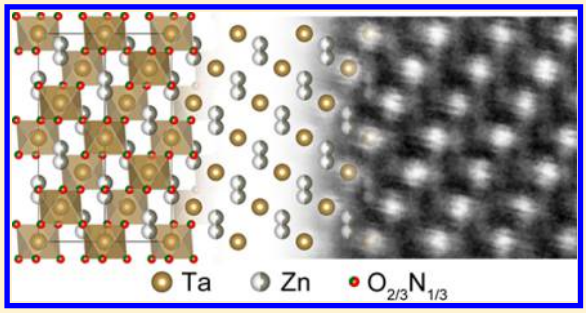

INTRODUCTION

ABO_3 oxides with a $LiNbO_3$-type (LN-type) structure have been of great academic and industrial importance owing to their ferroelectricity, piezoelectricity, photoelasticity, and nonlinear optical polarizability.[1] Unlike perovskite oxides, the LN-type structure ($R3c$ space group) does not necessarily require second order Jahn−Teller (SOJT) active d^0 cations (e.g., Ti^{4+}, Nb^{5+}, and Ta^{5+})[2] or lone pair electrons (e.g., Pb^{2+} and Bi^{3+})[3] to show these properties. A large electric polarization of LN-type oxides originates from a strong Coulomb repulsion between A and B cations across the shared octahedral face (Figure 1a). Recent discoveries of multiferroic properties in $ScFeO_3$[4] and $FeTiO_3$[5] and a ferroelectric-like transition in metallic $LiOsO_3$[6] have expanded interest in this structural type.

It is well-established that the ferroelectric transition in $BaTiO_3$ perovskite is classified as displacive type, with a displacement of Ti^{4+} from the ideal position below a Curie temperature T_c.[7] By contrast, the mechanism underlying the ferroelectric transition in $LiNbO_3$ (T_c = 1470 K)[8] and $LiTaO_3$ (T_c = 940 K)[9] is, despite their wide range of industrial applications, still under intensive debate. A high-temperature paraelectric phase (HTLN-type structure) above T_c adopts an $R\bar{3}c$ space group with the B cation located at a centrosymetric 6*b* site (Figure 1b). Regarding the position of the A cation, two models have been proposed, relevant to a displacive type and an order−disorder-type transition.[8−10] Experimentally, Raman spectroscopy and infrared reflectivity measurements suggested the displacive type with A cation of the high-temperature phase at a 6*a* site,[11] while results of neutron and Raman scattering measurements are in favor of the order−disorder type with A cation at a disordered 12*c* site with a 50% occupancy (Figure

Received: August 18, 2016
Published: November 18, 2016

DOI: 10.1021/jacs.6b08635
J. Am. Chem. Soc. 2016, 138, 15950−15955

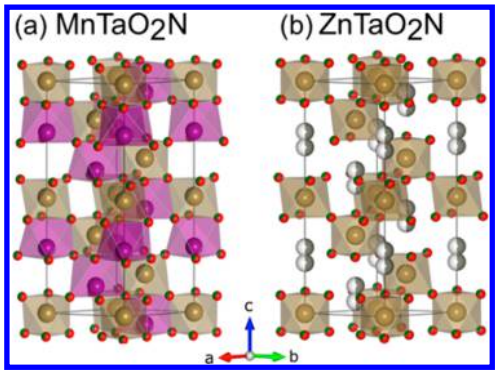

Figure 1. Structures of (a) $MnTaO_2N$ with LN-type structure ($R3c$)[17] and (b) $ZnTaO_2N$ with HTLN-type structure ($R\bar{3}c$). Gray, brown, purple, red, and green balls represent Zn, Ta, Mn, O, and N.

1b).[12] From the theoretical side, a phonon analysis supported the order−disorder mechanism,[13] but a molecular dynamics study suggested a *compromised* scenario involving a displacive-type transition for the B cation and an order−disorder-type one for the A cation.[14] The difficulty in unveiling the transition mechanism in $LiNbO_3$ and $LiTaO_3$ is obviously related to very high T_c's. Although a recently discovered metallic system $LiOsO_3$ has T_c = 140 K, the electron−lattice coupling is supposed to provide substantial contributions to the transition.[6,15] Stabilization of the HTLN-type phase will allow one to study the transition mechanism.

Oxynitrides have attracted considerable attention because of various intriguing properties. For example, high permittivity observed in $BaTaO_2N$ and $SrTaO_2N$ with the perovskite structure was discussed in terms of tantalum displacements driven by high covalency in the Ta−N bonds (vs Ta−O bonds).[16] We have recently reported on a high-pressure synthesis of a LN-type oxynitride $Mn^{2+}Ta^{5+}O_2N$ with a novel helical spin order due to competing magnetic interactions of Mn^{2+} moments.[17] Here, we report on the high-pressure synthesis of the Zn analogue, $Zn^{2+}Ta^{5+}O_2N$, and its structural characterizations by means of powder synchrotron X-ray diffraction (SXRD), neutron diffraction (ND), and high-angle annular dark field scanning transmission electron microscopy (HAADF-STEM). Unlike $MnTaO_2N$, it adopts a HTLN-type structure, being stable (at least) down to 20 K, thus offering a unique opportunity to comprehensively understand the stability of the HTLN-type structure as well as the phase relation with the LN-type structure, without involving thermal effects.

■ EXPERIMENTAL SECTION

A polycrystalline sample of $ZnTaO_2N$ was synthesized by high-pressure reaction using ZnO and TaON. TaON was synthesized by heating Ta_2O_5 (99.99%, Rare Metallic) at 850 °C for 15 h in flowing dry ammonia gas at a rate of 20 mL/min. ZnO (99.9%, Rare Metallic) and TaON were weighed in a stoichiometric ratio and mixed thoroughly in air. Then, the mixture was pelletized, charged into a platinum capsule, put into a high-pressure cell (pyrophyllite), and heated at 1600 °C under 6 GPa using a cubic anvil press. After the sample was pressed to a target pressure and heated to a target temperature in 15 min, the temperature was stabilized for 1 h, and then quenched to room temperature within 5 min, followed by a slow release of the pressure.

The XRD data of the obtained product showed the formation of a rhombohedral phase with cell parameters of a = 5.23 Å and c = 14.09 Å, but it contained a large amount of impurity phases including TaON (18.6 wt %) and $ZnTa_2O_6$ (2.4 wt %) as shown in Figure S1. Varying reaction temperature, pressure, and time failed to reduce the amount of impurity. However, when excess ZnO was used, the TaON impurity was drastically reduced. The best quality was achieved in the case of 50% excess of ZnO. Although we could not eliminate a small amount of TaON (3.5 wt %) and $ZnTa_2O_6$ (2.9 wt %), unknown peaks disappeared after the sample was washed with HCl for 2 h at 80 °C (Figure S2). The X-ray energy dispersive spectroscopy (EDS) of the sample after wash gave the Zn/Ta molar ratio of 1.04 for the main phase (Figure S3).

A whole solid solution series of $(Zn_{1-x}Mn_x)TaO_2N$ ($0 < x < 1$) was synthesized in a similar way, using TaON, ZnO, and MnO (99.9%, Rare Metallic) under 5.5 GPa at 1600 °C. The obtained samples were also washed with HCl.

To identify crystalline components of products, we measured powder XRD patterns at room temperature on a Bruker D8 Advance diffractometer equipped with a Cu Kα source. For structural refinement, SXRD experiments were conducted at room temperature on a Debye−Scherrer camera at the BL02B2 beamline at SPring-8 (λ = 0.42023 Å). NPD data were collected at 20 and 300 K using a Cu(311) or Ge(311) monochromator (λ = 1.5401 and 2.0775 Å, respectively) on BT-1 at NIST Center for Neutron Research (NCNR). Structural refinements were carried out using JANA2006.[18] Cation composition of the materials was studied with the energy dispersive X-ray (EDX) using an Oxford X-act detector mounted on a Hitachi S-3400N scanning electron microscope. The sample for transmission electron microscopy was prepared by dispersing the powder in ethanol and depositing a few drops of the dispersion on a holey carbon TEM grid. Electron diffraction (ED) patterns were collected on an FEI Tecnai G2 electron microscope operating at 200 kV. High-resolution high-angle annular dark field scanning transmission electron microscopy (HAADF-STEM) images were acquired on a probe aberration corrected FEI Titan^3 80-300 electron microscope operated at 300 kV. Optical second harmonic generation (SHG) was tested for ungraded powders at room temperature using a pulsed Nd:YAG laser (λ = 1064 nm, pulse duration 25 ps, repetition rate 10 Hz) as the light source.

First-principles calculations were performed using the projector augmented wave method as implemented in the VASP code.[19] The exchange-correlation term was treated with the Perdew−Burke−Ernzerhof functional.[20] The plane-wave cutoff energies were set to 550 eV, and integration in reciprocal space was performed with a 6 × 6 × 2 Γ-point centered mesh. The calculations were performed at 0, 6, and 20 GPa. The atoms on the 12c site in the HTLN-type structure were set to 6a sites in the initial structures. The O−N configurations in both LN- and HTLN-type structures were considered disordered by special quasirandom structure (SQSs).[21] The SQSs were constructed considering the ninth nearest neighboring pairs of the anion sublattice.

■ RESULTS AND DISCUSSION

The XRD pattern of the new rhombohedral phase is quite similar to that of LN-type $MnTaO_2N$ (Figure 1a).[17] The observed reflection conditions indicate that the space group is either polar $R3c$ or nonpolar $R\bar{3}c$. Thus, we initially assumed the LN-type structure ($R3c$) and carried out Rietveld refinement of SXRD data, placing Ta and Zn at the 6a (0, 0, z) site (where z = 0 and $z \sim 0.28$, respectively) and O at the 18b (x, y, z) site. Nitrogen was not taken into consideration at this stage because of little difference between the X-ray atomic scattering factors of oxygen and nitrogen. The isotropic thermal parameter U_{iso} of each atom was fixed to 3.0×10^{-3} Å^2.

The Rietveld refinement appeared to be converged with agreement factors of R_{wp} = 8.87% and GOF = 3.98. However, when isotropic thermal parameters were allowed to vary, a very large value of $U_{iso} = 35 \times 10^{-3}$ Å^2 was obtained for Zn. Inclusion of anisotropic thermal parameters gave a slightly better result (R_{wp} = 8.53%, GOF = 3.83), but U_{33} for Zn dictating a displacement along the c axis was too large (48×10^{-3} Å^2). Moreover, the z coordinate of 0.0794(3) for O

DOI: 10.1021/jacs.6b08635
J. Am. Chem. Soc. 2016, 138, 15950−15955

locates Ta almost at the center of octahedron, i.e., Ta−O = 2.001 Å (×3) and 2.072 Å (×3). It means that Ta^{5+} feels a negligible electrostatic repulsion from the countercation Zn^{2+} in the adjacent face-shared octahedra, which is distinct from known LN-type compounds having much larger off-center displacements of the B site (e.g., Ta−O = 1.99 Å (×3) and 2.11 Å (×3) for $MnTaO_2N$). From these results, we conclude that the LN-type structure is unlikely.

Accordingly, the SXRD data was refined with the HTLN-type structure ($R\bar{3}c$) placing Ta at 6*b* (0, 0, 0), Zn at 12*c* (0, 0, *z*) (where *z* ∼ 0.28) with an occupation factor of *g* = 1/2, and O at 18*e* (*x*, 1/3, 1/12), as shown in Figure 2a. We obtained

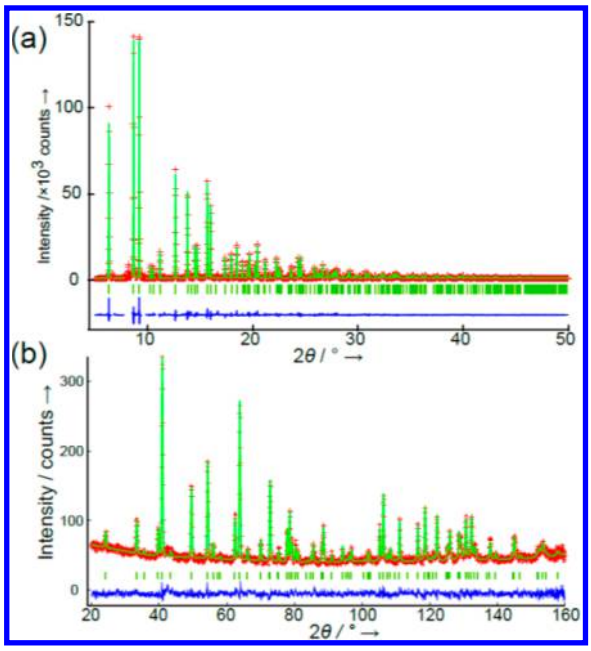

Figure 2. Rietveld refinement of (a) SXRD and (b) ND data for $ZnTaO_2N$ at room temperature (RT). Red crosses, green and blue lines, and green ticks represent observed, calculated, difference intensities, and Bragg peak positions, respectively.

better reliability factors of R_{wp} = 7.67% and GOF = 3.53, and the obtained isotropic thermal parameters are in an acceptable range. The resulting site occupancy of the mixed anion position is g_O = 1.002(8), corresponding to a nearly stoichiometric composition of $ZnTa(O,N)_{3.006(24)}$. No off-stoichiometry was observed for both cationic sites, while refining cation antisite disorder did not improve the result. The refinement with Zn at the "ideal" 6*a* site (in ZnO_3 triangular coordination) gave an enormously large U_{iso} of 38 × 10^{-3} $Å^2$. The Rietveld analysis using powder ND data was also performed assuming the HTLN-type structure (Figure 2b). The oxygen and nitrogen atoms were found to be randomly distributed at the 18*e* site. The O/N occupancy was constrained to be unity, and the isotropic thermal parameters of O and N were set to be equal. As a result, we obtained a nearly stoichiometric composition of $ZnTaO_{2.04}N_{0.98(2)}$. The refined parameters of SXRD and ND are summarized in Table 1. Bond valence sum (BVS) calculations[22] gave reasonable valences of +1.83 for Zn and +4.80 for Ta. A similar result was obtained for $MnTaO_2N$ (*V*(Mn) = +1.98, *V*(Ta) = +4.72).

The crystal structure analysis of $ZnTaO_2N$ is fully corroborated by transmission electron microscopy. The ED patterns (Figure 3a−c) can be completely indexed on a trigonal

Table 1. Structural Parameters of $ZnTaO_2N$ from Rietveld Refinement on SXRD and ND Data at 300 K

atom		300 K (SXRD)	300 K (ND)
	a/Å	5.23103(3)	5.23104(5)
	c/Å	14.0971(1)	14.1051(3)
Zn	*g*	0.5	0.5
	z	0.2828(1)	0.2829(2)
	U_{iso} (100 $Å^2$)	1.19(3)	1.15(8)
Ta	*g*	1	1
	U_{iso} (100 $Å^2$)	0.76(1)	0.64(4)
O/N	*g*	1	0.674/0.326(4)
	x	0.0384(8)	0.0365(2)
	U_{iso} (100 $Å^2$)	1.3(1)	0.98(3)
	R_{wp}/%	8.39	5.71
	R_p/%	5.74	4.60
	GOF	3.86	1.26

[a]Space group $R\bar{3}c$ (No. 167), *Z* = 6, with atoms in the following positions: Zn, 12*c* (0, 0, *z*); Ta, 6*b* (0, 0, 0); O(N), 18*e* (*x*, 1/3, 1/12).

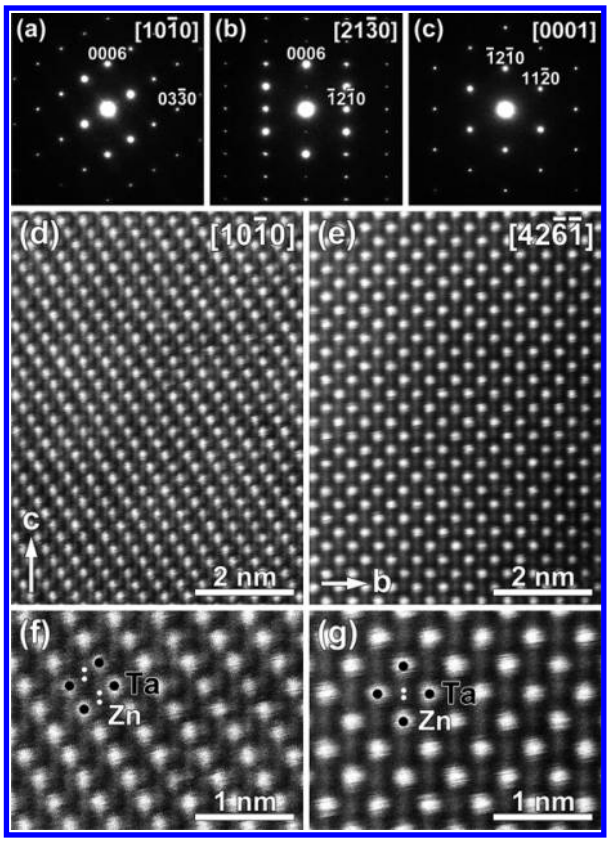

Figure 3. (a−c) ED patterns of $ZnTaO_2N$. (d−g) High-resolution HAADF-STEM images highlighting splitting of the Zn atomic positions.

*R*3*c* lattice. High-resolution HAADF-STEM images (Figure 3d,e) confirm the refined atomic arrangement. In these images, the intensity is proportional to the average atomic number of the projected columns. The Ta columns appear as bright sharp dots, while the intensity of the Zn columns is weaker and the splitting of the Zn positions gives rise to the characteristic intensity smearing along the *c* direction (Figure 3f,g). Notably, the absence of any extra reflections and/or structured diffuse intensity in the ED pattern indicates that the Zn displacements from the "ideal" 6*a* sites are random, without noticeable short-range correlations.

DOI: 10.1021/jacs.6b08635
J. Am. Chem. Soc. 2016, 138, 15950−15955

SHG was tested at room temperature for an ungraded powder of $ZnTaO_2N$. No SHG response was observed, consistent with the nonpolar ($R\bar{3}c$) structure (Figure 4b).

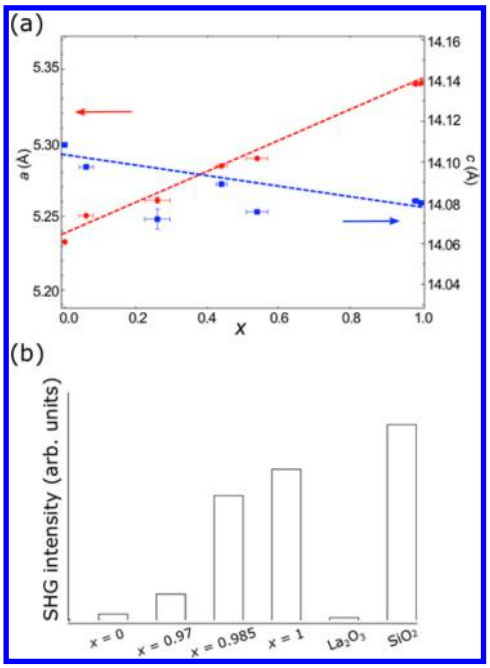

Figure 4. (a) Cell constants of $(Zn_{1-x}Mn_x)TaO_2N$. (b) SHG intensities for x = 0, 0.97, 0.985, 1. For comparison, we plotted results of La_2O_3 ($P\bar{3}m1$) and SiO_2 ($P3_121$).

Note that a tiny (nonzero) response comes from the surface (where the inversion symmetry is broken), which is inevitable for a powder specimen. Furthermore, the SXRD data at 20 K was also refined with the HTLN-type structure (Figure S4), meaning that, unlike $LiNbO_3$ and $LiTaO_3$, $ZnTaO_2N$ does not experience any structural transition. Annealing the quenched $ZaTaO_2N$ at 300 and 500 °C for 1 day did not induce any structural change. The low-temperature stabilization of the HTLN-type structure indicates that a thermal factor is not the cause of disordering of the A cations from the 6*a* site in the basal anion layer, supporting the order−disorder scenario for $LiNbO_3$ and $LiTaO_3$.

The local coordination geometry in $ZnTaO_2N$ is illustrated in Figure 5a. The Ta atom is located exactly at the center of the octahedron with the equidistant Ta−(O,N) of 2.031 Å, which is close to those of LN-type compounds with Ta^{5+}: 1.909 and

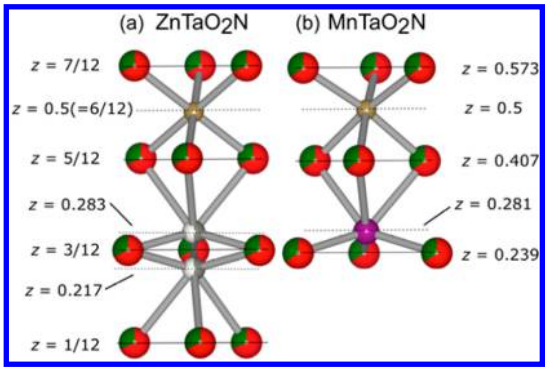

Figure 5. Coordination environment around A and B sites in (a) $ZnTaO_2N$ and (b) $MnTaO_2N$.[17]

2.073 Å (av 1.991 Å) in $LiTaO_3$[23] and 1.987 and 2.105 Å (av 2.046 Å) in $MnTaO_2N$.[17] On the other hand, the coordination environment of the ZnO_4N_2 octahedron is quite unusual, consisting of three short (1.992 Å) and three long (2.505 Å) bonds. This highly anisotropic octahedral coordination geometry (or a quasi-triangular coordination) makes a striking contrast to those found in zinc-containing LN-type oxides (Figure 5b) such as $ZnTiO_3$ (2.005 and 2.269 Å),[24] $ZnSnO_3$ (2.041 and 2.310 Å),[25] and $ZnPbO_3$ (2.020 and 2.278 Å).[26]

For $ZnTaO_2N$ and all the reported compounds of the LN-type[4−6,8,9,15,23−26] or HTLN-type[5,13,14] structures, we calculated an AO_6 octahedral distortion parameter, Δ, using the following equation[27]

$$\Delta = \frac{1}{6}\sum_{i}\left(\frac{d_i - d_{av}}{d_{av}}\right)^2 \quad (1)$$

where d_i is the individual bond length and d_{av} is the average length, and the result is represented in Table S1. It is clearly seen that Δ for ZnO_4N_2 is 1.30×10^{-2} at 300 K, which is far larger than those of any other LN- and HTLN-type compounds, for example, $\Delta = 0.362 \times 10^{-2}$ for MnO_4N_2 in $MnTaO_2N$,[17] $\Delta = 0.381 \times 10^{-2}$ for $ZnTiO_3$,[24] $\Delta = 0.503 \times 10^{-2}$ for $ZnSnO_3$,[25] and $\Delta = 0.360 \times 10^{-2}$ for $ZnPbO_3$.[26]

So far, we have demonstrated that $ZnTaO_2N$ crystallizes in the HTLN-type structure with Zn at the disordered site, and this "high-temperature" form is kept to low temperatures. This fact and the presence of the isovalent $MnTaO_2N$ with the LN-type structure allow us to seek for factors to stabilize the HTLN-type structure for $ZnTaO_2N$ (and LN-type for $MnTaO_2N$). We consider that the difference in structure mainly arises from the difference in electron count between Zn (d^{10}) and Mn (d^5). While a half-occupied d-shell in Mn^{2+} hybridizes with O/N 2p orbitals and favors octahedral coordination, Zn^{2+} with a fully occupied d-shell utilizes the empty 4s and 4p orbitals, allowing a considerable distortion from ZnO_4N_2 octahedral symmetry to form a quasitriangular ZnO_2N coordination. Such a distortion may also be supported by the coordination preference of the tetrahedral form for Zn^{2+}, relative to Mn^{2+}.[27] However, this cannot be a sole factor since $ZnM^{4+}O_3$ (M = Sn, Ti, Pb) species adopt the LN-type structure as well. It is hence considered that the occupation of the B site by pentavalent Ta, due to the O^{2-}/N^{3-} replacement (with respect to $ZnMO_3$), also contributes to the stabilization of the HTLN-type structure. The greater Coulomb repulsion between A^{2+}/B^{5+} cations (compared with A^{2+}/B^{4+}) across the shared octahedral face pushes Zn^{2+} far away from the octahedral center, eventually favoring the HTLN-type structure (along with the A site disorder).

As seen in Figure 1, both LN- and HTLN-type ABO_3 structures are viewed as heavily distorted perovskites with the antiphase rotation of corner-shared BO_6 octahedra along the [111] direction (denoted as $a^-a^-a^-$ in the Glazer notation) so as to accommodate a small A cation.[28] In general, the degree of octahedral rotation reduces with increasing temperature. In $CaTiO_3$, for example, the tilting system changes from $a^-b^+a^-$ to $a^0a^0c^-$ at 1498 K and to $a^0a^0a^0$ at 1634 K.[29] In $LiNbO_3$, the rotation angle reduces from ω = 23.3° at 300 K (LN phase) and 20.48° at 1470 K (HTLN phase).[30] Interestingly, the rotation angle of TaO_4N_2 octahedra in $ZnTaO_2N$ at room temperature is approximated as 24.3° which is larger than 22.5° in $MnTaO_2N$.[17] The reason for this opposite trend is not clear yet, but given the fact that octahedral tilting in perovskite

DOI: 10.1021/jacs.6b08635
J. Am. Chem. Soc. 2016, 138, 15950−15955

oxides has been mostly discussed for an ionic A cation favoring a more symmetrical environment, a directional or covalent-like bonding in Zn−(O,N) may lead to a less symmetrical environment and enhance the rotation angle.[31] We also checked the tilting behavior for $ZnTaO_2N$ and $MnTaO_2N$, revealing that the TaO_4N_2 octahedral tilting in the HTLN phase of $ZnTaO_2N$ increases upon cooling (ω = 24.9° at 20 K), which is a typical behavior in ABO_3 perovskite. On the other hand, for $MnTaO_2N$, the TaO_4N_2 octahedral tilting remains unaltered down to 20 K, within the experimental error. The suppressed tilting for the latter may be related to the effect from the face-sharing MnO_4N_2.

We prepared a solid solution $(Zn_{1-x}Mn_x)TaO_2N$ ($0 < x < 1$) to examine the relation between the two structural types, as a function of chemical composition. As in the x = 0 phase, a certain excess of Zn is always necessary to reduce impurity phases except for x = 1 (see laboratory XRD patterns in Figure S5). Thus, the Zn/Mn ratio was determined by EDS (Table S2). Figure 4a shows that the a axis decreases while the c axis increases with x. SXRD refinements revealed that samples with x = 0.06, 0.26, 0.46, and 0.54 adopt the HTLN-type form (Figures S6−S9). Strong SHG response is observable only for x = 0.985 and 0.99 (and 1), indicating that the HTLN-type phase is stable over a wide x range (Figure 4b). Remarkably, only 3% Zn substitution for Mn induces a centrosymmetric-to-non-centrosymmetric transition, implying the LN-type structure in $MnTaO_2N$ is close in energy to the HTLN-type. In order to compare the stability of these two structures, we conducted first-principles calculations for both end members (x = 0 and 1) at various pressures using a 30-atom supercell, where the O/N atoms were disordered by special quasirandom structures.[32] It is found that energy differences between LN- and HTLN-type structures at ambient pressure are fairly small (7 and 34 meV/f.u. for x = 0 and 1) (Figure S10), supporting experimental observations. We observed a tendency that the relative energy of the HTLN-type structures decreases with increasing pressure, and for $ZnTaO_2N$ the HTLN-type structure becomes stable at 20 GPa.

CONCLUSION

Using a high-pressure method, we have prepared a new oxynitride $ZnTaO_2N$. It crystallizes in a novel HTLN-type structure, with Zn sitting on the disordered 12c site. This structure shows a remarkable stability down to low temperatures, in contrast to reported HTLN-type compounds, enabling us to investigate the phase stability (vs LN-type) without thermal effects. It turned out that the stabilization of the HTLN-type structure arises from the closed d-shell of Zn^{2+} (affording the nearly triangular ZnO_2N coordination) and a strong electrostatic repulsion of Zn^{2+} and Ta^{5+}, a situation that is possible only with an oxynitride with the total negative charge of −7. Furthermore, only 3% Zn-for-Mn substitution in $MnTaO_2N$ induces a transition from the LN- to the HTLN-type structure. Together with the previous study,[17] this study domenstrates that the high-pressure reaction is advantageous for the synthesis of oxynitrides contaning middle-to-late transition metals. We believe that a number of oxynitrides such as $TMTaO_2N$ and $TMNbO_2N$ (e.g., TM = Fe^{2+}, Co^{2+}, Ni^{2+}) could be prepared in the future, which offers further possibilities to tune the phase transition between LN- and HTLN-type structures.

ASSOCIATED CONTENT

Supporting Information

The Supporting Information is available free of charge on the ACS Publications website at DOI: 10.1021/jacs.6b08635.

Experimental details and additional charaterization data and images (PDF)

AUTHOR INFORMATION

Corresponding Author

*kage@scl.kyoto-u.ac.jp

ORCID

Koji Fujita: 0000-0002-1700-0889
Dmitry Batuk: 0000-0002-6384-6690
Hiroshi Kageyama: 0000-0002-3911-9864

Notes

The authors declare no competing financial interest.

ACKNOWLEDGMENTS

The authors would like to thank Tsukasa Matsubara for his support during an SHG measurement. This work was supported by CREST project and JSPS Grant-in-Aid for Scientific Research (A) (25249090 and 24248016), Young Scientists (B) (16K17877), and for Scientific Research on Innovative Areas "Nano Informatics" (26106514) and "Mixed Anion" (JP16H6439, JP16H6440, JP16H6441). The synchrotron radiation experiments were performed at the BL02B2 of SPring-8 with the approval of the Japan Synchrotron Radiation Research Institute (JASRI) (Proposal 2015B1110, 2015B1111, 2015B1472).

REFERENCES

(1) (a) OK, K. M.; Chi, E. O.; Halasyamani, P. S. *Chem. Soc. Rev.* **2006**, *35*, 710. (b) Rao, C. N. R.; Sundaresan, A.; Saha, R. *J. Phys. Chem. Lett.* **2012**, *3*, 2237.

(2) (a) Halasyamani, P. S.; Poppelmeier, K. R. *Chem. Mater.* **1998**, *10*, 2753. (b) Kunz, M.; Brown, I. D. *J. Solid State Chem.* **1995**, *115*, 395. (c) Halasyamani, P. S. *Chem. Mater.* **2004**, *16*, 3586.

(3) (a) Catalan, G.; Scott, J. F. *Adv. Mater.* **2009**, *21*, 2463. (b) Shirane, G.; Pepinsky, R.; Frazer, B. C. *Acta Crystallogr.* **1956**, *9*, 131.

(4) Kawamoto, T.; Fujita, K.; Yamada, I.; Matoba, T.; Kim, S. J.; Gao, P.; Pan, X.; Findlay, S. D.; Tassel, C.; Kageyama, H.; Studer, A. J.; Hester, J.; Irifune, T.; Akamatsu, H.; Tanaka, K. *J. Am. Chem. Soc.* **2014**, *136*, 15291.

(5) Varga, T.; Kumar, A.; Vlahos, E.; Denev, S.; Park, M.; Hong, S.; Sanehira, T.; Wang, Y.; Fennie, C. J.; Streiffer, S. K.; Ke, X.; Schiffer, P.; Gopalan, V.; Mitchell, J. F. *Phys. Rev. Lett.* **2009**, *103*, 047601.

(6) Shi, Y.; Guo, Y.; Wang, X.; Princep, A. J.; Khalyavin, D.; Manuel, P.; Michiue, Y.; Tsuda, K.; Yu, S.; Arai, M.; Shirako, Y.; Akaogi, M.; Wang, N.; Yamaura, K.; Boothroyd, A. T.; Sato, A. *Nat. Mater.* **2013**, *12*, 1024.

(7) (a) Cochran, W. *Adv. Phys.* **1960**, *9*, 387. (b) Harada, J.; Axe, J. D.; Shirane, G. *Phys. Rev. B* **1971**, *4*, 155.

(8) Boysen, H.; Altorfer, F. *Acta Crystallogr., Sect. B: Struct. Sci.* **1994**, *50*, 405.

(9) Abrahams, S. C.; Buehler, E.; Hamilton, W. C.; Laplaca, S. J. *J. Phys. Chem. Solids* **1973**, *34*, 521.

(10) (a) Ridah, A.; Fontana, M. D.; Bourson, P. *Phys. Rev. B: Condens. Matter Mater. Phys.* **1997**, *56*, 5967. (b) Lines, M. E. *Phys. Rev.* **1969**, *177*, 819. (c) Safaryan, F. P. *Phys. Lett. A* **1999**, *255*, 191. (f) Inbar, I.; Cohen, R. E. *Phys. Rev. B: Condens. Matter Mater. Phys.* **1996**, *53*, 1193.

(11) (a) Johnston, W. D.; Kaminow, I. P. *Phys. Rev.* **1968**, *168*, 1045. (b) Servoin, J. L.; Gervais, F. *Solid State Commun.* **1979**, *31*, 387.

DOI: 10.1021/jacs.6b08635
J. Am. Chem. Soc. 2016, 138, 15950−15955

(12) (a) Chowdhury, M. R.; Peckham, G. E.; Saunderson, D. H. *J. Phys. C: Solid State Phys.* **1978**, *11*, 1671. (b) Jayaraman, A.; Ballman, A. A. *J. Appl. Phys.* **1986**, *60*, 1208.
(13) Parlinski, K.; Li, Z. Q.; Kawazoe, Y. *Phys. Rev. B: Condens. Matter Mater. Phys.* **2000**, *61*, 272.
(14) (a) Phillpot, S. R.; Gopalan, V. *Appl. Phys. Lett.* **2004**, *84*, 1916. (b) Sanna, S.; Schmidt, W. G. *IEEE Trans. Ultrason. Ferroelectr. Freq.Control.* **2012**, *59*, 1925.
(15) (a) Sim, H.; Kim, B. G. *Phys. Rev. B: Condens. Matter Mater. Phys.* **2014**, *89*, 201107. (b) Liu, H. M.; Du, Y. P.; Xie, Y. L.; Liu, J. -M.; Duan, C.-G.; Wan, X. *Phys. Rev. B: Condens. Matter Mater. Phys.* **2015**, *91*, 064104. (c) Giovannetti, G.; Capone, M. *Phys. Rev. B: Condens. Matter Mater. Phys.* **2014**, *90*, 195113.
(16) (a) Kim, Y.-I.; Woodward, P. M.; Baba-Kishi, K. Z.; Tai, C. W. *Chem. Mater.* **2004**, *16*, 1267. (b) Zhang, Y.-R.; Motohashi, T.; Masubuchi, Y.; Kikkawa, S. *J. Eur. Ceram. Soc.* **2012**, *32*, 1269.
(17) Tassel, C.; Kuno, Y.; Goto, Y.; Yamamoto, T.; Brown, C. M.; Hester, J.; Fujita, K.; Higashi, M.; Abe, R.; Tanaka, K.; Kobayashi, Y.; Kageyama, H. *Angew. Chem., Int. Ed.* **2015**, *54*, 516.
(18) Petříček, V.; Dušek, M.; Palatinus, L. *Z. Kristallogr. - Cryst. Mater.* **2014**, *229*, 345.
(19) (a) Blöchl, P. E. *Phys. Rev. B: Condens. Matter Mater. Phys.* **1994**, *50*, 17953. (b) Kresse, G.; Joubert, D. *Phys. Rev. B: Condens. Matter Mater. Phys.* **1999**, *59*, 1758. (c) Kresse, G.; Hafner, J. *Phys. Rev. B: Condens. Matter Mater. Phys.* **1993**, *47*, 558. (d) Kresse, G.; Furthmüller, J. *Comput. Mater. Sci.* **1996**, *6*, 15.
(20) Perdew, J. P.; Burke, K.; Ernzerhof, M. *Phys. Rev. Lett.* **1996**, *77*, 3865.
(21) Zunger, A.; Wei, S.; Ferreira, L.; Bernard, J. *Phys. Rev. Lett.* **1990**, *65*, 353.
(22) (a) Brown, I. D.; Altermatt, D. *Acta Crystallogr., Sect. B: Struct. Sci.* **1985**, *B41*, 244. (b) Brese, N. E.; O'Keeffe, M. *Acta Crystallogr., Sect. B: Struct. Sci.* **1991**, *B47*, 192.
(23) Abrahams, S. C.; Bernstein, J. L. *J. Phys. Chem. Solids* **1967**, *28*, 1685.
(24) Inaguma, Y.; Aimi, A.; Shirako, Y.; Sakurai, D.; Mori, D.; Kojitani, H.; Akaogi, M.; Nakayama, M. *J. Am. Chem. Soc.* **2014**, *136*, 2748.
(25) Inaguma, Y.; Yoshida, M.; Katsumata, T. *J. Am. Chem. Soc.* **2008**, *130*, 6704.
(26) Yu, R.; Hojo, H.; Mizoguchi, T.; Azuma, M. *J. Appl. Phys.* **2015**, *118*, 094103.
(27) Morkoç, H.; Özgür, Ü. *Zinc Oxide: Fundamentals, Materials and Device Technology*; Wiley, 2009.
(28) (a) Woodward, P. M. *Acta Crystallogr., Sect. B: Struct. Sci.* **1997**, *53*, 32−43. (b) Megaw, H. D. *Acta Crystallogr., Sect. A: Cryst. Phys., Diffr., Theor. Gen. Crystallogr.* **1968**, *24*, 583.
(29) Kennedy, B. J.; Howard, C. J.; Chakoumakos, B. C. *J. Phys.: Condens. Matter* **1999**, *11*, 1479.
(30) Abrahams, S. C.; Levinstein, H. J.; Reddy, J. M. *J. Phys. Chem. Solids* **1966**, *27*, 1019.
(31) Glazer, A. M. *Acta Crystallogr., Sect. B: Struct. Crystallogr. Cryst. Chem.* **1972**, *28*, 3384.
(32) Zunger, A.; Wei, S.-H.; Ferreira, L. G.; Bernard, J. E. *Phys. Rev. Lett.* **1990**, *65*, 353.

DOI: 10.1021/jacs.6b08635
J. Am. Chem. Soc. 2016, 138, 15950−15955